ELSEVIER

Contents lists available at ScienceDirect

## Materials Science & Engineering A

journal homepage: www.elsevier.com/locate/msea



# On the strain rate sensitivity of aluminum-containing transformationinduced plasticity steels: Interplay between TRIP and TWIP effects



K. Li<sup>a</sup>, V.S.Y. Injeti<sup>a</sup>, R.D.K. Misra<sup>a,\*</sup>, Z.H. Cai<sup>b</sup>, H. Ding<sup>b</sup>

- a Department of Metallurgical, Materials and Biomedical Engineering, University of Texas at El Paso, 500 W. University Avenue, El Paso, TX 79968-0521, USA
- <sup>b</sup> Department of Materials Science and Engineering, Northeastern University, Shenyang 110819, China

#### ARTICLE INFO

# Keywords: Steels Strain rate Electron microscopy Deformation behavior

#### ABSTRACT

The primary objective of the study is to elucidate the effect of strain rate on the deformation behavior of Alcontaining transformation-induced plasticity steels (TRIP) via combination of depth-sensing nanoindentation experiments and post-mortem analyses of deformed steels using transmission electron microscopy (TEM). The strain rate sensitivity decreased with increased Al-content. The activation volume of 2Al-steel was  $\sim$  half (6b³) of 6Al-steel (11b³), where b is the magnitude of the Burgers vector. The strain rate influenced the evolution of strain-induced martensite (TRIP effect), dislocation slip and deformation twinning (TWIP effect). The interplay between TRIP and TWIP effects as a function of strain rate is analyzed and discussed in terms of the three internal energies, namely  $\gamma \rightarrow \alpha$  (austenite $\rightarrow$ martensite) transformation Gibbs free energy, strain energy and stacking fault energy. These were impacted by the Al-content of the steels, which altered the austenite stability and propensity to deformation twinning. The study provides insights into the design of next generation of TRIP steels for the fabrication of automotive components.

#### 1. Introduction

Automotive industry continues to demand high performance materials that are formable and facilitate ease of manufacture of automotive components and can withstand impact during the collision. Additionally, from the view point of energy conservation and environmental protection, high strength-high ductility combination and light-weight materials are preferred in the automotive industry. Thus, the current focus is on advanced high strength and low density steels to reduce vehicle weight, and increased passenger safety. Transformationinduced plasticity (TRIP) steels have the potential to exhibit excellent combination of specific strength and ductility [1-3]. During plastic deformation, the retained austenite phase is transformed to martensite contributing to increased work hardening and enhancing the ductility. To obtain low density, light elements such as aluminum and magnesium are being added to TRIP steels. However, the presence of metastable retained austenite in the microstructure can lead to a complex mechanical behavior as compared to stable phases. A number of studies [4–7] have proven that aluminum added to medium-Mn (5–12%) TRIP steels can facilitate the aforementioned desired properties to be obtained. For instance, Fe-5Mn-0.2C (wt%) steel was characterized by both high tensile strength (850-950 MPa) and high ductility (20-30%) [4]. Similarly, high tensile strength (1018 MPa) and high elongation

(31%) was obtained in Fe-7Mn-0.1C (wt%) steel [5]. High tensile strength of 1420 MPa and elongation of 31% was obtained in Fe-7Mn-0.2C (wt%) steel [6]. On the other hand, steel containing 1.5 wt% Al (Fe-10Mn-0.14C-1.5Al) exhibited tensile strength of 1095 MPa and elongation of 42% [7].

Studies on strain rate effects are currently limited, particularly in steels that contain Al. Bleck and Schael [8] and Van Slyeken et al. [9] illustrated increased work hardening with increased strain rate with the ability for high energy absorption. However, the observations made by of Pychmintsev et al. [10] were in striking contrast to those made by Beck and Schael [8] and Van Slyeken et al. [9]. Thus, the strain rate effects continue to be unclear and require attention.

We recently studied factors that govern structure-property relationship in hot-rolled and cold-rolled medium-Mn TRIP steels containing Al [11,12]. In sequel to the previous studies, we elucidate have the impact of strain rate in Al-containing TRIP steels on the mechanical stability of austenite and solid-state phase transformation of austenite into martensite, and discuss the behavior in terms of Gibbs energy, strain energy and stacking fault energy.

#### 2. Experimental: materials and methods

The nominal chemical composition of experimental steels with

E-mail address: dmisra2@utep.edu (R.D.K. Misra).

<sup>\*</sup> Corresponding author.

Table 1 Chemical composition of the three experimental steels (in wt%).

Steel	С	Mn	Al	Fe
Fe-11Mn-0.2C – 2Al	0.22	11.2	1.95	86.63
Fe-11Mn-0.2C – 4Al	0.18	11.02	3.81	84.99
Fe-11Mn-0.2C – 6Al	0.21	10.75	6.08	82.96

different Al-content is listed in Table 1 and the processing of steels is described elsewhere [11,12]. In brief, 40 kg experimental steel ingots were cast in a vacuum induction furnace. Subsequently, these ingots were heated at 1200 °C for 2 h, hot forged into rods of section size  $100 \text{ mm} \times 30 \text{ mm}$  and air cooled to room temperature. Next, the forged rods were soaked at 1200 °C for 2 h, hot-rolled to 4 mm thick strip in the temperature range of 1150-850 °C, and air cooled to room temperature.

The as-hot-rolled sheets were subjected to quenching and tempering heat treatment instead of austenite reverted transformation for reasons discussed elsewhere [13-16]. They were first annealed in the intercritical temperature range for 1 h, followed by quenching in water to room temperature. Subsequently, the quenched samples were tempered at 200 °C for 20 min and air cooled to ambient temperature. During tempering, carbon diffuses from ferrite to austenite and is expected to increase the stability of austenite, providing superior ductility.

To study the microstructure, the samples were etched with 25% sodium bisulfite solution and examined using optical microscope (OM) and scanning electron microscope (SEM). Tensile properties are revisited here. Room temperature tensile tests were conducted on specimens of dimensions 12.5 mm width and gage length of 50 mm at a constant crosshead speed of 3 mm min<sup>-1</sup>. The tensile specimens were machined from the heat-treated steel with tensile axis parallel to the rolling direction. The volume fraction of austenite phase was determined by X-ray diffraction (XRD) using CuK<sub>\alpha</sub> radiation and involved the use of integrated intensities of  $(200)_{\alpha}$  and  $(211)_{\alpha}$  peaks and those of  $(200)_{\gamma}$ ,  $(220)_{\gamma}$  and  $(311)_{\gamma}$  peaks. The volume fraction of austenite  $V_A$ was estimated using equation [17]:

$$V_A = 1.4I_{\gamma}/(I_{\alpha} + 1.4I_{\gamma}) \tag{1}$$

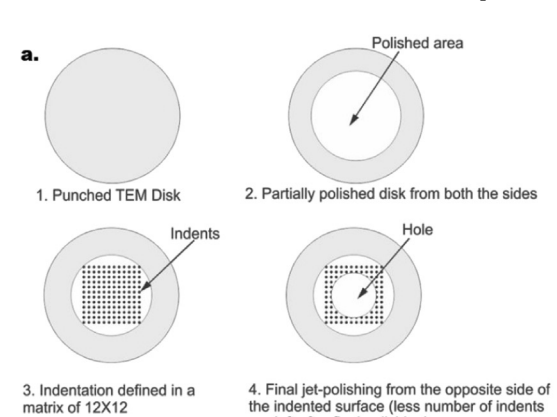
where  $I_{\gamma}$  is the integrated intensity of austenite and  $I_{\alpha}$  is the integrated intensity of  $\alpha$ -phase.

Strain rate experiments were conducted using nanoindenter for the following reasons [18-23]. In nanoindentation experiments, the diameter of the indenter tip (20 nm) is very small to produce a highlystressed volume beneath the indenter. During nanoscale deformation experiment, the fundamental deformation-induced processes in a small volume of the material has a low probability of encountering pre-existing dislocations prior to the nanoscale deformation. Intriguingly, nanoscale deformation experiments enable us to study phase transformation and evolution of microstructure via post-mortem electron

microscopy of the plastically deformed region [23].

Keeping in mind that the plastically deformed region surrounding the indentation was to be subsequently examined by TEM, the approach adopted consisted of the following steps. In the first step, the 3 mm disks were punched from the experimental steels that were initially thinned to  $\sim 35-40 \, \mu m$  thickness. To ensure that the nanoindents were present along the thin area of the disk for study via TEM, a modification of twin-jet electropolishing developed by our group was adopted and is illustrated elsewhere [23]. The second step involved partially jet electropolishing of the 3 mm disks in a refrigerated electrolyte consisting of 10% perchloric acid in acetic acid at 25 V for  $\sim$  30 s to obtain a shining surface in the center part of the 3 mm disk, prior to nanoindentation experiments. Next, the electropolished disks were subjected to nanoindentation experiments in displacement-controlled mode at strain rates in the range of 0.01-1/s. The maximum displacement was set to 200 nm. The nanoindenter system (Keysight Technologies) consisted of a Berkovich three-sided pyramidal diamond indenter with a nominal angle of 65.3° and indenter tip diameter of 20 nm. An array of indentation (12  $\times$  12) were made with the indent gap of 20  $\mu$ m. Once the indentation experiment was complete, the disks were removed from the mount and final jet polishing was carried out from the side opposite to the indented surface to minimize the electropolishing away of the indents. Using this developed approach, the area surrounding the indentation, which is present around the final jet-polished hole, was electron transparent to study the deformation behavior at different strain rates using TEM (Hitachi H7600, 200 kV). A schematic illustration of the experimental procedure including sample preparation for nanoindentation experiments and subsequent examination of the plastic zone surrounding the indentation by TEM is reproduced here in Fig. 1.

Small indentations are expected to have a strain-gradient distribution within the plastic zone surrounding the indentation. Thus, the aim was to focus on obtaining the specifics of deformed structure by TEM from the center of the plastic zone of each of the experimental steels. Here the electron beam and/or sample is moved in small steps from the region close to the tip of the indenter to the area where the deformation was almost absent. This procedure enables us to locate the approximate center of the plastic zone. Thus, the evolution of deformation structure described below can be assumed to be the area from a region close to the center of the plastic zone. The displacement for the three experimental steels at the strain rates studied was in the narrow range of ~ 150-200 nm. A number of experiments were carried out at each strain rate, followed by post-mortem analysis by TEM. The data was carefully analyzed and confirmed for reproducibility of the "deformation data (i.e., strain rate data)" and "indentation-induced deformation structures". Furthermore, during post-mortem TEM analysis, the primary focus was on studying the deformation of austenite in terms of TRIP and TWIP effects.



are left after final polishing).

matrix of 12X12

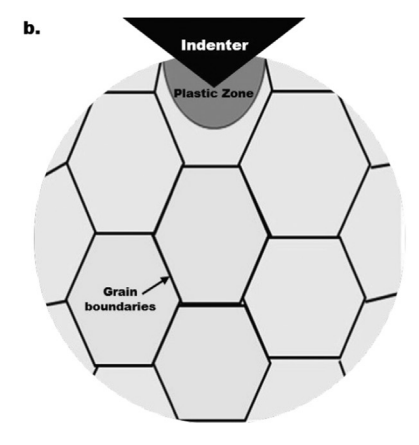


Fig. 1. (a) Schematic illustration of experimental jetpolishing procedure for nanoindentation experiments, and (b) nanoindentation performed in the center of an austenite grain.

### Download English Version:

# https://daneshyari.com/en/article/7974334

Download Persian Version:

https://daneshyari.com/article/7974334

<u>Daneshyari.com</u>